The measurement of atmospheric CO_2 at KMA/GAW regional stations, the characteristics, and comparisons with other East Asian sites

Haeyoung Lee [1,2], Sang-Ok Han[1], Sang-Boom Ryoo[1], Jeong-soon Lee[3], and Gang-woong Lee[2]

1 Environmental Meteorology Research Division, National Institute of Meteorological Sciences, Jeju, 63568, Republic of Korea
2 Atmospheric Chemistry Laboratory, Hankuk University of Foreign Studies, Gyeonggi-do, 17035, Republic of Korea
3.Korea Research Institute of Standards and Science, Daejeon, 34113, Republic of Korea

Correspondence to Haeyoung Lee (leehy80@korea.kr)

Abstract. To understand the carbon cycle at policy-relevant spatial scales, a high density of high-quality CO_2 measurement sites is needed. In 2012, the Korea Meteorological Administration (KMA) installed CO_2 monitoring systems at Anmyeondo (AMY) in west, Jeju Gosan Suwolbong (JGS) in south-west and Ulleungdo (ULD) in east parts of Korea. Three stations were instrumented with identical greenhouse gas measurement systems based on Cavity Ring Down Spectroscopy (CRDS) and a new drying system developed by KMA and Korea Research Institute of Standards and Science (KRISS). This drying system is suitable in the humid areas; water vapour measured by the CRDS in ambient air was 0.001 to 0.004% across the stations. Measurement uncertainties expressed by the quadrature sum of the uncertainties from the drying system, scale propagations, repeatability, and reproducibility were ~ 0.11 ppm from all KMA stations in 68% confidence interval. Average monthly CO_2 enhancements above the local background at each station were 4.3 ± 3.3 ppm at AMY, 1.7 ± 1.3 ppm at JGS and 1 ± 1.9 ppm (1σ) at ULD respectively during 2012 to 2016. At AMY station, located between China and Korea, CO_2 annual means and seasonal variations are also greater than the other KMA stations indicating that it is affected not only by local vegetation, but also added anthropogenic sources. Selected baseline CO_2 at AMY and at JGS in the west part of Korea are more sensitive to East Asia according to wind direction and speed. Through the comparison of long-term trends and growth rates at AMY with other East Asian stations over 15 years, it was suggested that they could be affected by not only local vegetation but also measurement quality.

1. Introduction

Carbon dioxide, the most important anthropogenic greenhouse gas, is one of the main drivers of climate change on Earth. Measurements of atmospheric CO_2 have assumed increased importance to track the increase in global CO_2 due to fossil fuel combustion (Canadell et al., 2007; Knorr, 2009).

Roughly half of anthropogenic CO_2 emitted by fossil fuel combustion is stored in the atmosphere, whereas the other half is absorbed by the oceans and terrestrial ecosystems. Recent studies showed the atmospheric CO_2 network is not yet dense enough to confirm or invalidate the increased global carbon uptake, estimated from ocean measurement or ocean models (Wanninkhof et al., 2012) but emphasized that the combination of a highly dense observation network, coupled with atmospheric models, leads to help understand regional carbon fluxes (Dolman et al., 2009). Therefore, confidence in our understanding of carbon cycle processes may be improved by a higher density of continuous measurement sites.

There are now over 400 regional stations monitoring atmospheric CO_2 under the Global Atmosphere Watch Programme (GAW) of the World Meteorological Organization (WMO) (https://gawsis.meteoswiss.ch). These sites capture more regional scale

information on fluxes than global stations, which reflect only well-mixed air mass. However, if technical measurement skill and data quality control are not sufficient, the data may not be useful to help identify and understand changes to the carbon cycle caused by climate change. Also, both measurement uncertainty and imperfect knowledge of the composition of background air can limit the precision of observation-based estimates of local or regional scale greenhouse gas enhancements (Graven et al., 2012; Turnbull et al., 2009, 2015).

Korea is important due to its location, where it is affected by flow from the Asia Continent, especially China. Korea's atmospheric CO_2 monitoring history started at Tae-Ahn Peninsula (TAP, 36°44'N, 126°08'E, 20 m above sea level), in the west part of Korea, in 1990 with weekly flask-air samples as a part of the NOAA/CMDL/GMD Cooperative Global Air Sampling Network (http://www.esrl.noaa.gov/gmd/ccgg/flask.php). Studies demonstrated its regional characteristically high CO_2 was affected by China's industrial regions, while for CH_4 it was affected by Russian wetlands and local rice cultivation near TAP (Dlugokencky et al., 1993; Kim et al., 2014).

Since 1999, the Korea Meteorological Administration (KMA) has been monitoring atmospheric CO_2 at Anmyeondo (AMY, 36.53°N, 126.32°E, 46 m above sea level from a 40 m tower), about 28 km from TAP. Nevertheless, this was the first attempt to continuously monitor CO_2 in Korea. In 2012, KMA expanded its monitoring network to include data from the south-west (Jeju Gosan Suwolbong, JGS, 33.30°N, 126.16°E) and the east (Ulleungdo, ULD, 37.48°N, 130.90°E) parts of Korea to cover the whole peninsula for a better understanding of CO_2 sources and sinks. At the same time, all three monitoring stations started to use analyzers based on Cavity Ring Down Spectroscopy (CRDS; a different model at each station, Picarro, CA, USA) with the same measurement method. So far, even though measurements began in 1999 at AMY, there is no published description of methods used to measure and process the data from the three KMA sites.

In this paper, we present the CO_2 measurement such as sampling system, data quality and processing methods at those three KMA monitoring stations. The measurement uncertainties are calculated separately from the hourly, daily and monthly standard deviations, which include natural variability and measurement uncertainty. We analyze the characteristics of CO_2 at KMA stations during 2012 to 2016 and compare the data to other stations in East Asia: the global background WMO/GAW station in Waliguan (WLG, 36.28°N, 100.90°E, 3810 m), China, and Ryori (RYO, 30.03°N, 141.82°E, 260 m), which reflects global growth rates as a regional WMO/GAW station in Japan (Watanabe et al., 2000).. In addition, we present 15 years of long-term CO_2 measurements in East Asia, including those from AMY. Furthermore, this paper will serve a reference for KMA data archived at the World Data Centre for Greenhouse Gases.

2.   Experiment

2.1   Sampling sites

The locations of Anmyeondo (AMY), Jejudo Gosan Suwolbong (JGS), and Ulleungdo (ULD) stations are shown in Fig. 1 with their details summarized in Table 1.

AMY is located in the west part of Korea, about 130 km southwest from the megacity of Seoul. Within a 100 km radius, the semiconductor industry and relevant industries exist. Also, the largest thermal power plants fired by coal and heavy oil in Korea are within 35 km to the north-east and south-east of the station. Local activity is related to agriculture, such as rice paddies, sweet potatoes and onions, while the area is also known for its leisure opportunities during summer. The west and south side of AMY is open to the sea and along the coast, there is a large tidal mudflat with many pine trees.

JGS is located in the west part of Jeju Island, which is the biggest volcanic island (1,845.88 km^2) in the south-west of Korea and about 90 km from the mainland. Jeju is popular for tourists regardless of the season, while the region of Suwolbong is famous as a Global Geo-park due to the outcrops of volcanic deposits exposed along the coastal cliff where JGS is located. In Jeju, there are two major power plants fired by heavy oil at approximately 47 km north-east and 16 km south-east from the stations. The side of the station from south-west to north-west is open to the sea, where there are volcanic basalt rocks. The sea to the south is connected to the East China Sea and the sea to the west is linked to the Yellow Sea. Next to JGS there is a wide plain where mainly potatoes, garlic and onions are harvested.

ULD is located in the east part of Ulleung Island, which is in the east part of Korea and about 155 km from the mainland. In south-east area of Korea Peninsula, there are very famous cities for steel, chemical, and petrochemical industries along the coast line and those cities are located about 200 – 250 km south-west from the island. Ulleung Island is 72 km^2, volcanic origin, and the rocky steep-sided island with top of a large stratovolcano reaching a maximum elevation of 984 m. This peak is located at north-west of ULD. There are a few small mountains whose heights are about 500 to 960 m a.s.l., within 5 km to the north and south-east of the station. Due to those geological features, ULD is mainly affected by airflow up over the hill from the south-west and downslope winds from north-east. There is also a small town in the valley northeast of the station with a small port, which is 810 m away from the station. In the south-west area, there is a small brickyard 200 m from the ULD. Farming and fishing industries are very active on the island, though there is no farm in the southern area.

An automatic weather station (AWS) was installed at AMY near the inlet, and 10 m above the station at JGS and ULD, but separate from the air inlet tower.

2.2 Measurement system: Inlet, drying system and instrument

The measurement system consists of three main parts: inlet, drying system and instruments (Fig. 2). The intake is an inverted stainless steel box (15 cm (W) x 25 cm (D) x 30 cm (H)) with a stainless steel filter (D 4.7 cm, pore size 5 µm) mounted on a plastic mesh holder and connected to the Dekabon sampling tubing (Nitta Moore 1300-10, I.D 6.8 mm, O.D 10 mm). Over times longer than one month, a significant pressure drop occurs between the inlet and the pump, so the filter is replaced monthly.

Sample air is dried with a system that has a cold trap (CT-90, Operon, Korea), which is connected to the pump (KNF N145.1.2AN.18, Germany, 55 L/min, 7 bar in AMY; KNF N035AN.18, Germany, 30 L/min, 4 bar in JGS and ULD). The cold trap is set to – 80 ℃ and keeps its temperature. When the sample air comes from outside into the drying system, the inner temperature increases. Therefore ambient air is cooled down to – 20 ℃ in the first chamber, and then to – 50 ℃ in the second chamber. To increase dehumidification efficiency, the second chamber is filled with stainless steel beads (Fig. 2).

One of the dual traps is used to dry ambient air for 24 hours while the other is warmed and drained. The dehumidification and water drain sequence is as follows: (step 1) pump/cold trap A is employed to dry ambient air for 24 hours (step 2) pump/cold trap B turn off to melt ice at ambient temperature for 20 hours (step 3) pump B turns on to pressurize and water drain for 2 hours (step 4) cold trap B turns on and cools to operating temperature for 2 hours (step 1) pump/cold trap B are employed drying ambient air. The difference between this system and a typical cryogenic one is that it was designed with a dual mode, with one trap drying while water is automatically drained from the other. Therefore it avoids the cold trap impinger clogging during long-term, unattended monitoring. This drying system was developed by KMA and Korea Research Institute of Standards and Science (KRISS) in 2011 for the remote monitoring stations so that it can be easily accessed remotely.

Even though the H_2O monitored by CRDS was not calibrated, hourly mean H_2O through the drying system is $0.004 \pm 0.005\%$ at AMY, $0.001 \pm 0.002\%$ in JGS and $0.001 \pm 0.004\%$ in ULD during 2012 to 2016. Laboratory standard gases prepared by the Central Calibration Laboratory (CCL), which is operated by the National Oceanic and Atmospheric Administration, Global Monitoring Division in Boulder, Colorado, USA, typically contain less than 0.0001% H_2O (www.esrl.noaa.gov/gmd/ccl/airstandard.html). When we sampled them directly to CRDS without this drying system, mean H_2O (10 min average) was 0.0009% regardless of the CO_2 level across the KMA monitoring stations.

For example, when there is a difference in H_2O at AMY between laboratory standard gases and ambient samples of 0.003%, this creates a small bias of 0.012 ppm on 400 ppm CO_2 according to the equation suggested by Rella et al. (2013):

$$\frac{C_{dilution}}{C_{dry}} = 1 - 0.01 H_{act} \tag{1}$$

where C is the CO_2 mole fraction and H_{act} is the actual water mole fraction (in %). Since working standards showed almost same level of H_2O to laboratory standards through the CRDS, we considered the CO_2 mole fraction dilution offsets between calibration standards and sample air when the uncertainty was estimated (sect 3.1).

After the drying system, ambient air flows through the 1/8" (o.d.) stainless steel tubing to an 8 port multi-position valve (VICI), which selects among standard gases and ambient air. A leak test of all lines is performed every month. CRDS is well-known for its highly linear and stable response (Crosson, 2008). A model G2301 (Picarro, USA) was installed in Oct, 2011, and it became our official CO_2 measurement at AMY starting January 1, 2012. Picarro models G1301 and G2401 have been used to measure ambient CO_2 and CH_4 since January 1 and February 12 in 2012, at JGS and ULD, respectively. Those analyzers monitor CO_2 every 5 sec across the KMA Greenhouse Gas (GHG) network.

At AMY, a non-dispersive infrared analyzer (NDIR, Ultramat 6, Siemens, Germany) was used to monitor atmospheric CO_2 every 30 sec from February 1, 1999 to December 31, 2011. During the period, we had three step dehumidification system, 1) - 4℃ cold trap 2) nafion and 3) $Mg(ClO_4)_2$, before installing the new system.

2.3 Calibration, quality control and data processing

2.3.1 Calibration method

The metrological definition of calibration is followed; operation that, under specified conditions, in a first step, establishes a relation between the quantity values with measurement uncertainties provide by measurement standards and corresponding indications with associated measurement uncertainties and, in a second step, uses this information to establish a relation for obtaining a measurement result for an indication (JCGM, 2012).

After starting to operate KMA GHG network in 2012, we calibrate our instruments against WMO-X2007 scale with our working standards. Our standard hierarchy consists of the laboratory standards from CCL, which are the highest rank in our network (https://www.empa.ch/web/s503/gaw_glossary), and working standards that are certified by the laboratory standards. 4 laboratory standards are prepared from 360 to 480 ppm with the uncertainty of ± 0.070 ppm (Zhao et al., 2006). Since AMY is a central lab for the GHG network, working standards used at three stations are filled and certified by laboratory standards with CRDS for CO_2 dry mole fraction at AMY. We have 4 working standards at each station from 360 to 460 ppm at intervals of 30 –

40 ppm with the uncertainty of ± 0.088 ppm after transferring the scale. This value is also used as the scale propagation factor of the measurement uncertainty in section 3.1.

Our ability to maintain and propagate the WMO-X2007 scale was shown through the 6th Round Robin comparison of standards hosted by the CCL (https://www.esrl.noaa.gov/gmd/ccgg/wmorr/wmorr_results.php, the difference of low level was 0.03±0.04 ppm while 0.04 ± 0.06 ppm for high CO_2), a comparison of continuous measurements with the traveling instrument of the World Calibration Centre (WCC-Empa, 2017(a), (b) and 2014.), and a co-located comparison of discrete samples collected at AMY and analyzed by NOAA/ESRL with our in situ analyzer results. This ongoing comparison between level 1 (L1) hourly data from the CRDS and weekly flask-air samples collected at AMY has been implemented since December, 2013. The mean difference between flask minus in situ is -0.11 ± 2.32 ppm from 2014 to 2016, close to GAW's compatibility goal for CO_2 in the Northern Hemisphere (± 0.1 ppm) (Fig 3).

The analyzers are calibrated every two weeks; all 4 working standard gases are sampled by CRDS for 40 min. The first 30 min of each cylinder run are rejected and 10 min are used for the calibration of CO_2 to ensure instrument stabilization. 4 standards are adequate to determine CO_2, as indicated by mean residuals of 0.0003 ± 0.026 ppm from a linear function fitted to the measurements of standards. Calibration connects analyzer response to the WMO-X2007 scale, and also tracks drift in the analyzer. The drift of the CRDS over two weeks is negligible indicating the mean values were ~ 0.006 ppm at AMY, ~ 0.001 ppm at JGS and ~ -0.019 ppm at ULD respectively. Therefore the calibrations are applied as a stepwise change fortnightly.

When we started monitoring atmospheric CO_2 with NDIR at AMY, it was calibrated every 2 hours with 4-point calibration tanks against KRISS scale from 1999 to 2011 Dec. During this period, we had used the cylinders which were certified by KRISS directly without working standards. KRISS and WMO scales agreed well in CCQM-P41 organized by the International Bureau of Weights and Measures (BIPM) (www.bipm.org/utils/common/pdf/final_report/QM/P41/CCQM-P41_part1.pdf).

.2.3.2 Data quality control process

All data are monitored, collected and stored at the Environmental Meteorological Research Division (EMRD), National Institute of Meteorological Sciences (NIMS) in Jeju, Korea. Raw data based on 5 second intervals are processed two ways: 1) auto flagging and 2) manual flagging. Auto flagging identifies instrument malfunction and instrument detection limit of CO_2. Auto flags are assigned when our algorithm detects deviations from prescribed ranges for analyser engineering data.

Acceptable values for the parameters related to instrument function are: H_2O (%) < 0.02; 139.95 < cavity pressure (Torr) < 140.05; and 44.99 < cavity temperature (℃) < 45.01. H_2O > 0.02% indicates periods when the drying system had problems or a leak in the gas line occurred, while the ranges of cavity pressure and temperature were suggested by the manufacturer. Instrument measurement range is based on the calibration range, from 360 to 460 ppm at 30 - 40 ppm intervals. Therefore flags are assigned when CO_2 is outside this range.

Manual flags are assigned by technicians at each station according to the logbook based on: inlet filter exchange, diaphragm pump error, low flow rate, dehumidification system error, calibration periods, experimental periods such as participation in comparison experiments, observatory environmental issue such as construction next to a station, extreme weather, or other issues related to the instrument. These codes refer to definitions by the World Data Centre for reactive gases and aerosols maintained by EBAS for the GAW Programme (http://www.nilu.no/projects/ccc/flags/flags.html) and were modified for the Korea network. Data with flags are reviewed by scientists at the EMRD, and valid data are selected as Level 1 (L1).

2.3.3 Regional background selection method

L1 data include local and long range transported pollution by human and/or biotic activities. Therefore, only those data that represent non-polluted and well-mixed air should be selected for analysis on a regional scale. The data are selected for background when they meet the following conditions: 1) Hourly averages are calculated when there are at least 60 30 sec measurements from the NDIR and at least 300 5 sec measurements from the CRDS, 2) the hourly average of level 1 has a standard deviation less than "A", 3) and the differences between consecutive hourly averages are less than "B". A and B were determined empirically and are equal. We determined 1.8 ppm for AMY, 1 ppm for JGS, and 0.8 ppm for ULD. This process selects 55% to 60% of the data at each station, and they are defined as Level 2 (L2) hourly data. To calculate daily averages (L2 daily), at least 6 L2 hourly data are required. In this paper, the smoothed curves fitted to L2 daily data is calculated with methods by Thoning et al. (1989) to represent the regional baseline as reducing noise due to synoptic-scale atmospheric variability and measurement gaps. Fig. 3 shows L1 hourly data, L2 daily data, and the smoothed curves fitted to L2 daily data.

2.3.4 Data availability

Our L2 hourly and daily data of AMY since 1999 and JGS since 2012, which are used for this paper, can be downloaded from World Data Centre for Greenhouse Gases (WDCGG, http://gaw.kishou.go.jp) under the WMO/GAW Programme. ULD data can be accessed through the same website in the near future.

3.   Results and Discussion

3.1   Measurement uncertainty

Variability in CO_2 observed at KMA's stations includes contributions from natural atmospheric variability and variability related to the air handling and measurement procedures. Natural atmospheric variability is represented, for example, by the standard deviation of all measurements contributing to a time-average, after the contribution of experimental noise is accounted for. Here we develop methods to calculate practical realistic measurement uncertainties. Based on measurements of target cylinders and a co-located comparison of measurements at AMY, we assume systematic biases are negligible. According to the previous studies, the total measurement uncertainty consists of multiple uncertainty components (Andrews et al., 2014, Verhulst et al., 2017). However, in this paper, we assess the measurement uncertainty based on the following components:

$$(U_T)^2 = (U_{h2o})^2 + (U_P)^2 + (U_r)^2 + (U_{scale})^2 \qquad (2)$$

where U_T is the total measurement uncertainty in the reported dry-air mole fractions; U_{h2o} is the uncertainty from the drying system; U_p is repeatability; U_r is reproducibility; and U_{scale} the uncertainty of propagating the WMO-XCO$_2$ scale to working standard gases.

U_{h2o} is computed from the differences in H_2O (%) between the ambient airstream through the drying system and standard gases injected directly, bypassing the drying system. According to the GAW recommendation, the standard gases should be treated through the same system to air sample (WMO, 2016). However, our drying efficiency is not constant so that we injected standard

gases directly as a reference value. Here, we define H_2O from the standard gases as 0.0009%. This value has been constant and stable during 2012 to 2016. On the other hand, the drying system efficiency is not constant so this uncertainty component is time dependent. Eq.(1) was applied for this factor where H_{act} is the difference between H_2O in samples and standard gases (0.0009%). Hourly CO_2 dilution offsets range from -0.05 to 0.09 ppm at AMY, -0.02 to 0.07 ppm at JGS and -0.05 to 0.08 ppm at ULD during 2012 to 2016. Since positive and negative values are found, we use following equation:

$$U_x = \sqrt{\frac{\sum_{i=1}^{N}(x_i)^2}{N}} \tag{3}$$

where U_x represents U_{h2o}; x is the hourly CO_2 dilution offsets from Eq(1); N is the total number of hourly mean values. U_{h2o} is tabulated for each station in table 2.

U_p is determined from the standard deviations of working standard measurements, as described in section 2.3.1 and expressed by a pooled standard deviation

$$U_p = \sqrt{\frac{\sum_{i=1}^{N} Ni \times Si^2}{Ni - Nt}} \tag{4}$$

where S_i is the standard deviation of 10 min averages of working standard measurements; N_i the number of data during 10 minutes (based 5 sec intervals); and N_t is the total number of calibrations during the period. S_i varied from 0.02 to 0.09 ppm at AMY, 0.02 to 0.07 ppm at JGS and from 0.01 to 0.05 at ULD. The pooled standard deviations (U_p) are shown in table 2.

U_r is the drift occurring between two-weekly calibration episodes, which was mentioned in section 2.3.1. We determined it as the differences in CO_2 measured from cylinders with subsequent calibrations over two weeks. It ranged from -0.08 to 0.1 ppm at AMY, -0.07 to 0.09 ppm at JGS and -0.16 to 0.11 ppm at ULD. We expressed U_r as the standard deviation of all drift values during the experimental period using Eq (3), where U_x represents U_r; x ΔCO_2 during 2 weeks; and N is the total number of data. They are tabulated with other uncertainty terms by site in table 2.

According to the Zhao et al.,(2006) the uncertainty of working standards can be calculated by the propagation error arising from the uncertainty of primaries with maximum propagation coefficient ($\gamma = 1$) and repeatability. Similarly U_{scale} for working standard is determined by

$$U_{scale} = \sqrt{U_p^2 + U_{lab}^2} \tag{4}$$

where U_{lab} is the uncertainty of laboratory standards, which CCL (NOAA/ESRL) certified. Here, U_{lab} has the same value as the uncertainty of Secondaries, 0.070 ppm, in the one-sigma absolute scale. These values are the same for all stations since they are calibrated by a central lab in AMY. Therefore U_p is the repeatability at AMY since we propagate the standard scale through the same anlayzer and set-up for the atmospheric monitoring.

In the future, quoted uncertainties could be greater due to including more error sources. Repeatability and reproducibility may become more precise with improvements in technologies and methods..

3.2 CO_2 data from 2012 to 2016 at KMA's three monitoring stations

The L1 hourly data, L2 daily data and smoothed curves fitted to L2 daily data are shown in Fig. 3. Episodes of elevated CO_2 were often observed at AMY, with a mean difference between maximum and minimum L1 hourly values in a year of ~102.1 ± 12.1 ppm; for the other sites, maximum minus minimum values were ~62.5 ± 9.2 ppm at JGS, and ~55.1 ± 9.6 ppm in ULD. The
5   enhancement relative to the local background mole fraction helps evaluate local additions of CO_2, with the excess signal defined as:

$$CO_{2XS} = CO_{2OBS} - CO_{2BG}$$

10   Where CO_{2OBS} is L1 hourly data and CO_{2BG} indicates regional background at the site, determined from the smoothed curve fitted to L2 daily data (section 2.3.3). When we roughly analyzed the foot prints for hourly CO_{2XS} at three stations, the potential source region was considered as not only Korean Peninsula but also from northern-eastern China (KMA, 2014). This happens due to synoptic system that developing low pressure over the source regions provide uplift the pollutions into the free troposphere and make them descent to downwind area (Tohjima et al., 2010, Tohjima et al., 2014, Lee et al., 2016).

15   Monthly mean CO_{2XS} at AMY was 4.3 ± 3.3 ppm, with 1.7 ± 1.3 ppm at JGS and 1.0 ± 1.9 ppm at ULD during 2012 to 2016. As described in section 2.1, since there are a lot of local activities around AMY, the mean value is larger than at other stations. It was assumed that CO_{2XS} is greater in winter compared to other seasons since photosynthesis is not active and respiration is diminished while anthropogenic sources such as residential sectors would dominate. However, all three stations showed highest CO_{2XS} in summer (JJA); it was 6.3 ± 4.9 ppm at AMY, 2.8 ± 1.4 ppm at JGS and 1.6 ± 2.7 ppm at ULD. Meanwhile the smallest
20   CO_{2XS} was during spring (MAM) at AMY with 2.8 ± 1.5 ppm, and during winter (DJF) at JGS and ULD with 0.9 ± 0.5 ppm and 0.4 ± 0.4 ppm respectively. Even though the selected data, which agree with the conditions given in 2.3.3, accounted for 55% to 60% of total data, the percentages are different according to the seasons. For example, during summer they decreased to 46% at AMY, 43% at JGS and 34% at ULD, meanwhile they account for 61% - 75% at all stations during winter. This means that since Korea Peninsula is affected by Siberian high from winter to spring with strong westerly wind, CO_{2OBS} was measured in well
25   mixed air relative to summer. Also, the wind speed decreased and diurnal variation increased during summer, so CO_{2OBS} might reflect local/regional sources and sink more than other seasons. We also discuss this issue in sections 3.3 and 3.4.

3.3 Local/regional effects on observed CO_2

To understand the influence of local surface wind on observed CO_2, bivariate polar plots were used. These plots are expressed by
30   dependence of all hourly CO_2 mole fractions (L1 data) on wind direction and speed in 2016 (Fig. 4 to 6). The wind data are derived from AWS which was described in section 2.1.

At AMY, lower CO_2 from autumn to winter occurred when winds mainly come from 315° to 360°. In spring, lower CO_2 started to include winds from 180° to 225° and the dominant wind direction shifted to the south (180° to 225°) in summer, indicating that lower CO_2 is linked to air masses from the sea (Yellow Sea). However, when wind speed is less than 5 m·s^{-1}, CO_2 is elevated
35   in all seasons and even in the sea-side. Especially in summer, this condition (wind speed < 5 m·s^{-1}) accounts for 80% of total data as indicating this might enhance CO_{2XS} in section 3.2. This also suggests that the high CO_2 can be observed in the air mass transported from not only Korea mainland but also west regions from western parts of Yellow sea.

JGS observed the strongest winds among the three stations for all seasons, with wind speed >7 m·s^{-1} occurring almost 36% of the time and a maximum speed up to ~40 m·s^{-1}. Lower CO_2 was observed with winds from 315° to 340° (Yellow Sea) and 120° to 160° (East China Sea) with wind speed > 5 m·s^{-1} regardless of seasons. In contrast, JGS is contaminated with local CO_2 emissions when wind comes from 45° to 135° with wind speed ≤ 5 m·s^{-1}. Since National Geo Park is east of the station, JGS could be affected by tourist activities such as transportations. The station is surrounded by farm lands so that it also could be affected by farming activities such as burning trashes and fields. High CO_2 was also observed with even strong wind, especially in Yellow sea side.

For ULD, the main wind directions are quite clearly from 0° to 90° (30%) and from 180° to 270° (33%), and wind speed less than 5 m·s^{-1} occurs 72% of the time. Normally lower CO_2 is monitored regardless of wind direction and wind speed. High CO_2 episodes were mainly observed when the wind sector was between 180° to 225°, presumably affected by the industry complex located in south –east part of Korea Peninsula and the brickyard, 200 m from the station. This wind direction is very dominant in summer with lower wind speed than other seasons.

Overall, both stations on the west side of Korea, AMY and JGS, might be more affected by continental air mass so their observations contain information about its sources and sinks, while they are also affected by local activities. Our eastern station, ULD, reflects lower CO_2 than other two stations with limited local activities. And it was also suggested that data from regional GAW stations have complex information, so it is necessary to develop a selection method for baseline conditions to better understand regional characteristics.

3.4   Average diurnal variation

Diurnal CO_2 variations, calculated as the average departure from the daily mean, in April, August, November and January, are used to represent the average diurnal variations in spring, summer, autumn and winter over 5 years in Fig 7. The standard deviations of the hourly means are ~ 16 ppm, ~ 7 ppm and ~ 5 ppm in AMY, JGS and ULD in January, April and November, but increased in August to ~ 20 ppm, ~10 ppm and ~ 8 ppm at AMY, JGS and ULD, respectively.

Prior studies described that diurnal variations can be influenced by atmospheric rectifier that is covariance between terrestrial ecosystem metabolism, such as an intensity of photosynthesis and a density of vegetation, and vertical atmospheric transports (Denning et al, 1999; Chan et al., 2008). Generally, rapid growth of turbulence at the surface after sunrise results in a high boundary layer and leads to decreased CO_2 measured at the station during daytime, while CO_2 accumulates in a stable nocturnal boundary layer created by a temperature inversion due to surface radiative cooling during the night (Higuchi et al., 2003). Also, the diurnal cycle in summer is the result of a combination of several factors, including active photosynthesis.

AMY and JGS showed those typical characteristics during all seasons, even though the differences between minimum and maximum CO_2 values significantly varied with month. However, ULD had this trend only in summer while other seasons showed very steady values through the day.

At AMY, the differences between maximum and minimum values were 13.5 ppm and 6.9 ppm in August and November, respectively, while those values were around 3 ppm in other seasons. This trend is very typical, as mentioned above. For JGS, those values were observed in the order of 9.6 ppm > 3.3 ppm > 2.8 ppm > 0.88 ppm in August, April, November and January, respectively. During summer, both AMY and JGS show an afternoon plateau in CO_2 from around mid-afternoon due to the combination of changes in the photosynthetic rate and increased boundary layer before sunset. In the evening CO_2 increases again when respiration dominates and the boundary layer becomes neutral or stable. Those two stations also show the clear wind

pattern such as land-sea breeze which might enhance the CO_2 diurnal cycle in summer. In contrast, at ULD, an average diurnal cycle was only obvious in August (peak to peak value of 3.9 ppm) and CO_2 increased monotonically during the afternoon. In other seasons, diurnal variations were 0.5~1 ppm.

For ULD the wind has no diurnal pattern differently from other two stations, however, come from certain sectors regardless of time, which we mentioned in section 2.1 and 3.3. ULD, at 221 m, is higher than AMY and JGS, so that it is less affected by local activities. Those geographical characteristics lead steady values at ULD except for summer that the most active photosynthesis.

3.5   Seasonal cycle and growth rates in East Asia

Seasonal variations from KMA's three stations and two other stations, WLG and RYO in East Asia, are compared in Fig. 8. WLG flask-air data from NOAA/ESRL/GMD and quasi-continuous measurements at RYO by Japan Meteorological Agency, which were downloaded from the World Data Centre for Greenhouse Gases (WDCGG), were fitted with smoothed curves and compared to KMA observations. It is known that the seasonal cycle of atmospheric CO_2 at surface observation stations in the Northern Hemisphere is driven primarily by net ecosystem production fluxes from terrestrial ecosystems (Tucker et al., 1986, Fung et al., 1987, Keeling et al., 1989). The averaged seasonal amplitude from 2012 to 2016 was smallest at WLG with 12.2 ± 0.9 ppm and largest at AMY with 15.4 ± 3.3 ppm. For JGS and RYO, peak to peak amplitudes were similar at 13.2 ± 1.7 ppm and 13.5 ± 1.6 ppm, whereas it was 14.2 ± 3.1 ppm at ULD (Table 3).

Normally, maximum CO_2 appears from 4.8 ppm at JGS to 5.8 ppm at AMY in April while the minimum appears in August between -6.8 at WGL to -9.6 ppm at AMY according to the station. The highest maximum and lowest minimum mean value appeared at AMY indicating that even though AMY is located at similar latitude as these other stations, it seems to capture photosynthetic uptake and respiration release of CO_2 by terrestrial ecosystems more than others. Also atmospheric CO_2 at AMY includes added anthropogenic emissions transported through the Yellow sea from the Asia Continent as explained in section 3.2 and 3.3. Meanwhile WLG is hardly affected by vegetation due to its altitude (Table 1).

The annual growth rate of CO_2, which was computed by the increase in annual means of de-seasonal trends from one year to the next at KMA sites, was quite similar to other East Asian stations and to the global growth rate from WMO (Fig.8 (b)). From 2012 to 2016, the average annual increase observed at all stations in East Asia was between 2.4 ± 0.7 and 2.6 ± 0.9 ppm/yr. This mean value is similar to the global increase of 2.21 ppm/yr from 2007 to 2016 reported by WMO (This value is determined by the absolute differences from previous year). The large increase in 2016 and 2015 was due to increased natural emissions of CO_2 related to the most recent El Niño event (Betts et al., 2016). Averaged annual CO_2 was highest at AMY and lowest at WLG among East Asian stations listed in Table 3, which shows that their differences are 8.5 ± 0.7 ppm. The low growth rate in 2014 at ULD might be caused by unusually low CO_2 in July-August 2014 resulting in no significant annual differences between 2013 and 2014 although the reasons are still unclear. Further studies are necessary to fully understand those results.

Since CO_2 is long-lived atmospheric species, the growth rate should be similar between the stations in the same region, even if they are subject to different combinations of anthropogenic and biogenic fluxes. However, our long term trends comparison showed that measurement and environmental changes also effected on its growth rate.

The long-term trends of CO_2 mole fractions at AMY, WLG and RYO from 2002 to 2016, which were extracted by the method of Thoning et al. (1989), are shown in Figure 9. The trends of CO_2 at WLG and RYO increased in parallel, whereas AMY increased

with a similar slope but with larger fluctuations than the other stations. Especially the negative growth rate, which was only observed in northern high latitude in 1992 due to Mount Pinatubo eruption, was recorded in 2004 and 2006 at AMY, while high growth rate was recorded in 2012 without ENSO (WDCGG, 2017; Stenchikov et al., 2002; Heimann and Reichetein, 2008).

In July 2004, the inlet height at AMY was changed from 20 m to 40 m above ground (Table 1); observed CO_2 mole fractions before moving the inlet height reflected more influence from local activities that affected the long-term trend (Song et al., 2005). According to the log book, in 2005 AMY was under the construction to expand the space with a new building that the instrument showed strong and highly localized signals during the period.

The measurement system such as instruments, drying systems and standard scale were changed in 2012 as described in section 2.2 and 2.3.1. It was proved that the CRDS has higher precision measurements than NDIR, and there were CO_2 offsets in a comparison between the two instruments (Chen et al., 2010; Zellweger et al., 2016). The maintaining traceability to the primary standard of the same scale under the GAW Programme would be more incentive to assure the long-term consistency (WMO, 2017).This result suggests that factors not only related to local sources/sinks, but also environmental changes around stations and level of technical skill are very important to monitor regional background CO_2 over the long term. On the other hand, on-going comparisons of measurements at co-located sites and for the same species, such as between discrete samples and continuous measurement (Masarie et al., 2001) are valuable means to maintain data quality and identify sampling issues rapidly. After 2012, long-term trends increased in parallel, with AMY 5.5 ± 0.3 ppm greater than RYO, and RYO 2.9 ± 0.3 ppm greater than WLG.

4.   Summary and Conclusions

Now many scientists are on the way to determine regional/national emissions through top-down methods with in situ data, so the importance of high density monitoring stations such as WMO/GAW regional stations is increasing since their data include a lot of information about CO_2 fluxes. In this regard, it remains a challenge for WMO/GAW stations to provide high quality data to better constrain emissions and sinks. In this paper we introduced the three KMA stations and measurement systems for high quality data, and we analyzed observed CO_2 characteristics with comparisons to other East Asia stations.

KMA instrumented three monitoring stations covering the Korean Peninsula in 2012 with a CRDS and a new drying system at each station. The drying system showed 0.001 to 0.004% water vapour in CRDS when sampling of ambient air, while it was 0.0009% in laboratory cylinders; those values satisfy GAW recommendation, 0.0039% (WMO, 2016). It also suggests the possibility to monitor atmospheric species in humid areas with easy maintenance and remote control of the system.

From 2012 to 2016, our measurement uncertainties, which include components of the drying system, measurement repeatability, reproducibility and scale propagation, are quite similar with 0.116 ppm, 0.114 ppm and 0.114 ppm at AMY, JGS and ULD respectively. In the future those uncertainties may increase as other components of uncertainty, and their variations over time, are added.

We assessed the CO_2 enhancement relative to local background level at each station; those were 4.3 ± 3.3 ppm at AMY while 1.7 ± 1.3 ppm at JGS and 1.0 ± 1.9 ppm at ULD during 2012 to 2016. This indicates that AMY has high CO_2 episodes compared to the other stations. The CO_2 mole fractions observed at AMY and at JGS in the west part of Korea are more sensitive to East Asia (e.g., China) according to wind direction and speed. Meanwhile they also reflect locally contaminated CO_2 under the stagnant conditions. At JGS, however, local anthropogenic emissions were very limited due to high wind speed and observed CO_2 levels are lower compared to AMY. The diurnal variations at these two stations indicate they reflect the impacts of local vegetation and

the degree and speed of atmospheric mixing. ULD, east of the Korean mainland, observed well-mixed air masses with small diurnal variations in CO_2 and similar CO_2 levels regardless of wind direction and speed due to its location.

The seasonal variation at AMY is large compared to the other stations in East Asia, indicating that it could be affected by not only vegetation but also anthropogenic emissions transported from Asia continent such as China. CO_2 observed at three KMA stations is higher than at WLG and similar to RYO as expected by their locations, while for growth rate, they are very similar to RYO and WLG during 2012 to 2016.

When AMY was compared to WLG and RYO in East Asia over 15 years, the long-term trend increased with a similar slope but with larger fluctuations compared to the other two stations. This seems to reflect not only carbon sources and sinks but also environment changes at the stations and level of sophisticated measurement expertise.

Since CO_2 observed in KMA includes much information about carbon fluxes in East Asia, these data are helpful to improve understanding of the carbon cycle in this region. In addition, to enhance the understanding of CO_2 observations at Korean monitoring stations, isotopes measurements such as ^{14}C in CO_2 would be very useful (Turnbull et al., 2011).

Acknowledgments. We would like to thank Dr. Edward Dlugokencky (NOAA/ESRL) for his helpful comments on this paper. We also thank Ryori station in Japan and Waliguan station in China for their data contributions. Finally we appreciate all staff and technicians at AMY, JGS, and ULD in Korea network. This work was funded by the Korea Meteorological Administration Research and Development Program "Research and Development for KMA Weather, Climate, and Earth system Services–Development of Monitoring and Analysis Techniques for Atmospheric Composition in Korea" under Grant (KMA2018-00522).

References

Andrews, A. E., J. D. Kofler, M. E. Trudeau, J. C. Williams, D. H. Neff, K. A. Masarie, D. Y. Chao, D. R. Kitzis, P. C. Novelli, C. L. Zhao, E. J. Dlugokencky, P. M. Lang, M. J. Crotwell, M. L. Fischer, M. J. Parker, J. T. Lee, D. D. Baumann, A. R. Desai, C. O. Stanier, S. F. J. De Wekker, D. E. Wolfe, J. W. Munger, P. P. Tans: CO_2, CO, and CH_4 measurements from tall towers in the NOAA Earth System Research Laboratory's Global Greenhouse Gas Reference Network: instrumentation, uncertainty analysis, and recommendations for future high-accuracy greenhouse gas monitoring efforts, Atmos. Meas. Tech., 7, 647-687, 2014

Betts, Richard A., Chris D. Jones, Jeff R. Knight, Ralph F. Keeling and John J. Kennedy: El Nino and a record CO2 rise. Nature Climate Change, 6, 806-810, 2016

Canadell, J. G., C. Le Que´re´, M. R. Raupach, C. B. Field, E. Buitenhuis, P. Ciais, T. J. Conway, N. P. Gilett, J. T. Houghton, and G. Marland: Contributions to accelerating atmospheric CO_2 growth from economic activity, carbon intensity, and efficiency of natural sinks, Proc. Natl. Acad. Sci. U. S. A., 104, 18,866 -18,870, doi:10.1073/pnas.0702737104, 2007

Chan, D., M. Ishizawa, K. Higuchi, S. Maksyutov, J. Chen.: Seasonal CO_2 rectifier effect and large-scale extratropical atmospheric transport, J.Geophys.Res., 113, D17309, doi:10.1029/2007JD009443, 2008.

Chen, H., J. Winderlich, C. Gerbig, A. Hoefer, C.W.Rella, E.R.Crosson, A.D.Van Pelt, J. Steinbach, O.Kolle, V.Beck, B.C.Daube, E.W.Gottlieb, V.Y.Chow, G.W.Santoni, and S.C.Wofsy.: High-accuracy continuous airborne measurement of greenhouse gases (CO_2 and CH_4) using the cavity ring-down spectroscopy (CRDS) technique, Atmos.Meas.Tech.,3,375-386, 2010.

Crosson, E.R.: A cavity ring-down analyzer for measuring atmospheric levels of methane, carbon dioxide, and water vapor, Appl.Phys. B, 92, 403-408, 2008.

Denning S., T. Takahashi, P. Friedlingstein.: Can a strong atmospheric CO2 rectifier effect be reconciled with a "reasonable" carbon budget?, Tellus, 51B, 249-253, 1999.

Dlugokencky E.J., J.M. Harris, Y.S. Chung, P.P. Tans, I. Fung.: The relationship between the methane seasonal cycle and regional sources and sinks at Tae-ahn Peninsula, Korea, Atmospheric environment, 2115-2120, 1993.

Dolman, A.J., C. Gerbig, J. Noilhan, C. Sarrat, and F. Miglietta: Detecting regional variability in sources and sinks of carbon dioxide: a synthesis, Biogeosciences, 1015-1026, 2009

Fung, I.Y., C.J. Tucker, and K.C.Prentice.:Application of advanced very high resolution radiometer vegetation index to study atmosphere biosphere exchange of CO_2, J.Geophys.Res., 92(D3), 2999-3015, 1987

Graven, H.D., Guilderson, T.P., and Keeling, R.F.: Observations of radiocarbon in CO_2 at La Jolla, California, USA 1992-2007: Analysis of the long-term trend, J.Geophys.Res.,117,D02302, https://doi.org/10.1029/2011JD016533, 2012

Higuchi, K., D. Worthy, D. Chan, and A. Shashkov: Regional source/sink impact on the diurnal, seasonal and inter-annual variations in atmospheric CO_2 at a boreal forest site in Canada, J. Tellus B: Chemical and Physical Meteorology 55, 2003

Heimann, M. and M. Reichstein: Terrestrial ecosystem carbon dynamics and climate feddbacks, Nature, 451 289-292, 2008

JCGM 200:2012: International vocabulary of metrology-Basic and general concepts and associated terms (VIM, 3rd edition, 2008 version with minor corrections), Available: https://bipm.org/utils/common/documents/jcgm/JCGM_200_2012.pdf, 2012

Keeling, C.D., R.B. Bacastow, A.F. Carter, S.C.Piper, T.P.Whorf, M. Heimann, W.G.Mook, and H.Roeloffzen: A three-dimensional model of atmospheric CO_2 transport based on observed winds: 1.Analysis of observational data in Aspects of Climate Variability in the pacific and the Western Americas, Geophys, Monogr. Ser., vol.55, edited by D.H. Peterson, pp.165-236, AGU, Washington, D.C.,1989

Kim H-S., Y-S Chung, P.P. Tans: A study on carbon dioxide concentrations and carbon isotopes measured in East Asia during 1991-2001, Air Qual Atmos Health, 173-179, 2014

KMA: Report of Global Atmosphere Watch 2013, Korea Meteorological Administration, 11-1360000-000991-10, 2014Knorr Wolfgang: Is the airborne fraction of anthropogenic CO_2 emissions increasing?, J.Geophys.Res., 36, L21710, doi:10.1029/2009GL040613, 2009

Lee, G., H-R Oh, C-H Ho, J. Kim, C-K Song, L-S Chang, J-B Lee, S. Lee: Airborne Measurements of High Pollutant Concentration Events in the Free Troposphere over the West Coast of South Korea between 1997 and 2011. Aerosol Air Qual.Res, 16, 1118-1130, 2016.

Masarie, K.A., R.L. Langenfelds, C.E. Allison, T.J. Conway, E.J. Dlugokencky, R.J. Francey, P.C. Novelli, L.P. Steele, P.P. Tans, B. Vaughn and J.W.C. White: NOAA/CSIRO, Flask Air Intercomparison Experiment: A Strategy for Directly Assessing Consistency among Atmospheric Measurements Made by Independent Laboratories, Journal of Geophysical Research, 106, 20445-20464, 2001.

Rella, C. W., Chen, H., Andrews, A. E., Filges, A., Gerbig, C.,Hatakka, J., Karion, A., Miles, N. L., Richardson, S. J., Steinbacher, M., Sweeney, C., Wastine, B., and Zellweger, C.: High accuracy measurements of dry mole fractions of carbon dioxide and methane in humid air, Atmos. Meas. Tech., 6, 837?860, doi:10.5194/amt-6-837-2013, 2013.

Song, B., K.J., Park, H.J. Yoo, and B.C. Choi: A comparative study on two consecutive years' CO_2 and CH_4 measurement from the different height of air sample inlet at KGAWO. Asia-Pacific Journal of Atmospheric Sciences, 41, 851-895, 2005

Stenchikov, G., A. Robock, V. Ramaswamy, M.D. Schwarzkopf, K. Hamilton, and S. Ramachandran: Arctic Oscillation response to the 1991 Mount Pinatubo eruption: Effects of volcanic aerosols and ozone depletion, J. Geophys.Res., 107, 4803, doi:10.1029/2002JD002090, 2002

Thoning K, W., P. P. Tans, and W. D. Komhyr: Atmospheric Carbon dioxide at Mauna Loa Observatory 2. Analysis of the NOAA GMCC Data, 1984-1985. J. Geophys.Res. 8549-8565, 1989

Tohjima, Y., H. Mukuai, S. Hashimoto, P. K. Patra: Increasing synoptic scale variability in atmospheric CO2 at Hateruma Island associated with increasing East-Asian emissions, Atmos.Chem.Phys., 10, 453-462, 2010

Tohjima, Y., M. Kubo, C. Minejima, H. Mukai, H. Tanimoto, A. Ganshin, S. Maksyutov, K. Katsumata, T. Machida, and K. Kita.: Temporal changes in the emissions of CH4 and CO from China estimated from CH_4 /CO_2 and CO/CO_2 correlations observed at Hateruma Island. Atmos.Chem.Phys., 14, 1663-1677, 2014

Tucker, C.J., I.Y. Fung, C.D. Keeling, and R.H.Gammon: Relationship between atmospheric CO_2 variations and a satellite-derived vegetation index, Nature, 319, 195-199, 1986

Turnbull, J.C., Rayner, P., Miller, J., Newberger, T., Ciais, P. and Cozic, A.: On the use of $^{14}CO_2$ as a tracer for fossil fuel CO_2: Quantifying uncertainties using an atmospheric transport model, J. Geophys. Res., 114, D22302, https://doi.org/10.1029/2009JD012308, 2009

Turnbull., J.C., Pieter P. T., Scott J. Lehman, David Baker, Thomas J. Conway, Y.S.Chung, Jay Gregg, John B. Miller, John R. Southon, and Ling-Xi Zhou: Atmospheric observations of carbon monoxide and fossil fuel CO_2 emissions from East Asia, J. Geophys. Res., 116, D24306, doi:10.1029/2011JD016691, 2011

Turnbull, J.C., Sweeney, C., Karion, A., Newberger, T., Lehman, S.J., Tans, P.P., Davis, K.J., Lauvaux, T., Miles, N.L., Richardson, S.J., Cambaliza, M.O., Shepson, P.B., Gurney, K., Patarasuk,R., and Razlivanoc, I.: Toward quantification and sources sector identification of fossil fuel CO_2 emissions from an urban area: Results from the INFLUX experiment, J.Geophys.Res.-Atmos., 120, 292-312, https://doi.org/10.1002/2014JD022555, 2015

Verhulst, Kristal R., Anna Karion, Jooil Kim, Peter K. Salameh, Ralph F. Keeling, Sally Newman, John Miller, Christopher Sloop, Thomas Pongetti, Preeti Rao1, Clare Wong, Francesca M. Hopkins, Vineet Yadav, Ray F. Weiss, Riley M. Duren, and Charles E. Miller: Carbon dioxide and methane measurements from the Los Angeles Megacity Carbon Project   Part 1: calibration, urban enhancements, and uncertainty estimates, Atmos. Chem. Phys., 17, 8313-8341, 2017.

Wanninkhof, R., Park, G.-H., Takahashi, T., Sweeney, C., Feely, R.,Nojiri, Y., Gruber, N., Doney, S. C., McKinley, G. A., Lenton,A., LeQuéré, C., Heinze, C., Schwinger, J., Graven, H., and Khatiwala, S.: Global ocean carbon uptake: magnitude, variabilityand trends, Biogeosciences, 10, 1983–2000, doi:10.5194/bg-10-1983-2013, 2013.

Watanabe Fumio, Osamu Uchino, Yasuhiko Joo, Masamich Aono, Keishirou Higashijima, Yoshiaki Hitano, Kazuhiro Tsuboi and Kazuto Suda, 2000, Interannual variation of growth rate of atmospheric carbon dioxide concentration observed at the JMA's three monitoring stations: Large increase in concentration of atmospheric carbon dioxide in 1998, Journal of the Meteorological Society of Japan, 78, 673-683, 2000

WMO: 18th WMO/IAEA Meeting on carbon dioxide, other greenhouse gases and related tracers measurement techniques (GGMT-2015), No.229, 2016

WMO: WMO Global Atmosphere Watch (GAW) Implementation Plan:2016-2023, No.228, 2017

WDCGG: WDCGG DATA SUMMARY, Greenhouse gases and other atmospheric gases, No.41, 2017

WCC-Empa: System and performance audit of methane and carbon dioxide at the regional GAW station Anmyeon-do Republic of Korea Jun, 14/2, pp 18, 2014

WCC-Empa: System and performance audit of surface ozone, carbon monoxide, methane, carbon dioxide and nitrous oxide at the regional GAW station Anmyeon-do Republic of Korea Jun, 17/1, pp 48, 2017 (a)

WCC-Empa: System and performance audit of surface ozone, carbon monoxide, methane, carbon dioxide and nitrous oxide at the regional GAW station Jeju-Gosan Republic of Korea Jun, 17/2, 2017 pp 42, 2017 (b)

Zhao, Cong Long and Tans, Pieter P. : Estimating uncertainty of the WMO mole fraction scale for carbon dioxide in air. Journal of Geophysical Research, 111, D08S09, doi:10.1029/2005JD006003, 2006

Zellweger Christoph, Lukas Emmenegger, Mohd Firdaus, Juha Hatakka, Martin Heimann, Elena Kozlova, T. Gerard Spain, Martin Steinbacher, Marcel V. van der Schoot, and Brigitte Buchmann.: Assessment of recent advances in measurement techniques for atmospheric carbon dioxide and methane observations, Atmos.Meas.Tech., 9, 4737-4757, 2016

(a)

(b)   (c)   (d)

Figure 1. Locations of (a) the three KMA monitoring stations in Korea, and Mt.Waliguan WMO/GAW global station and Ryori WMO/GAW regional station in East Asia. Surrounding Environment of the (b) Anmyeondo (AMY), (c) Jejudo Gosan Suwolbong (JGS), and (d) Ullengdo (ULD) station. Those figures are derived from Google map.
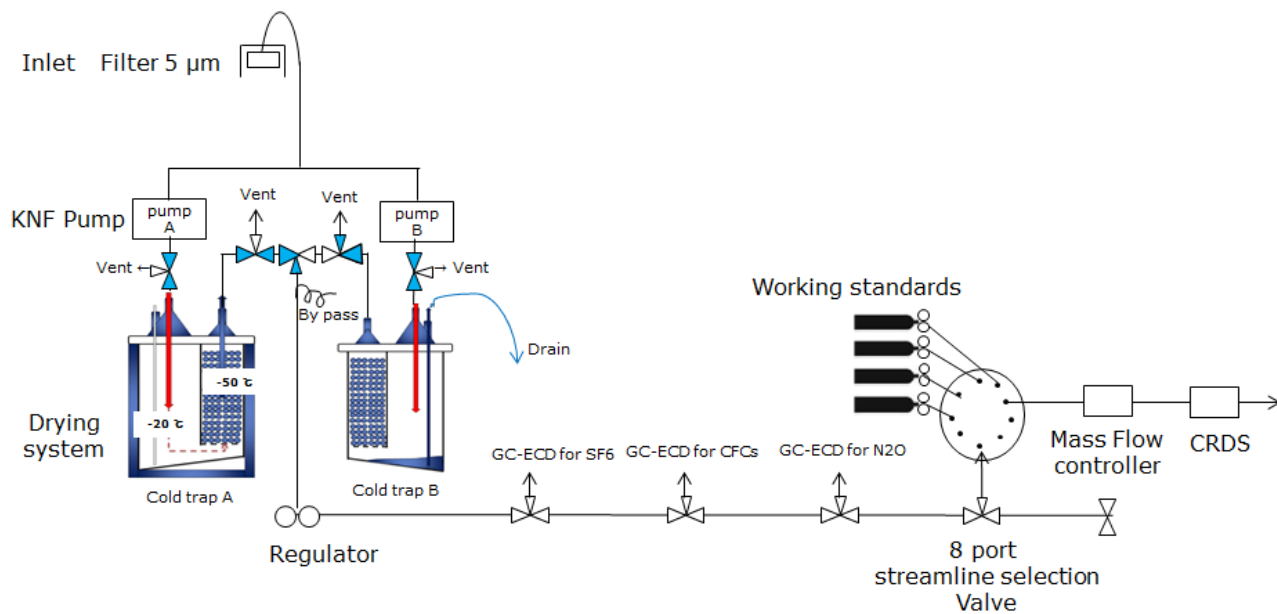
Figure 2. Schematic of the in-situ system when the drying system is at the state of step 3 in AMY, JGS and ULD.

(a)

(b)

(c)
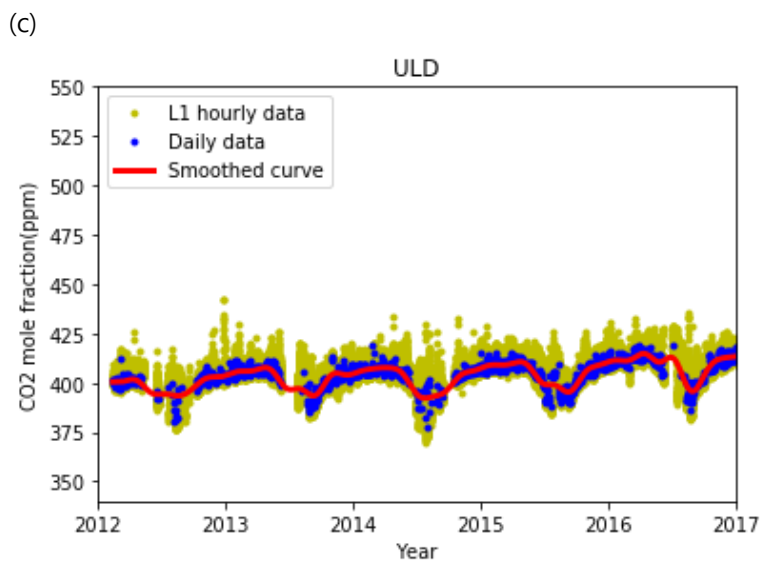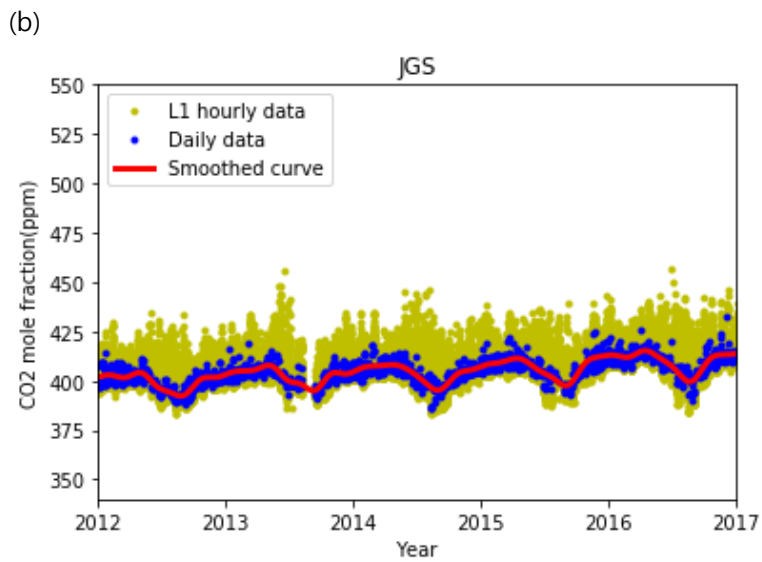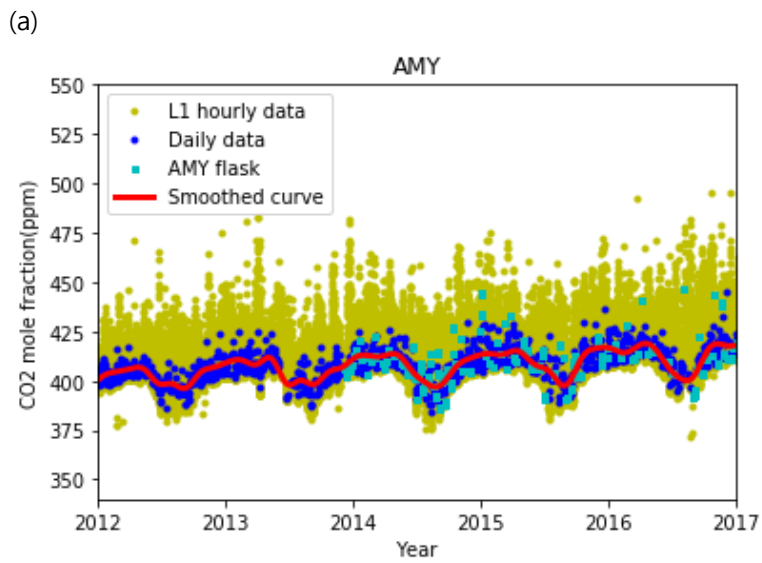
Figure 3. L1 hourly (yellow dots, CO_2 OBS), L2 daily (blue dots) averaged, and smoothed curves fitted to L2 daily averages (red line, CO_2 BG) at (a) AMY, (b) JGS and (c) ULD.
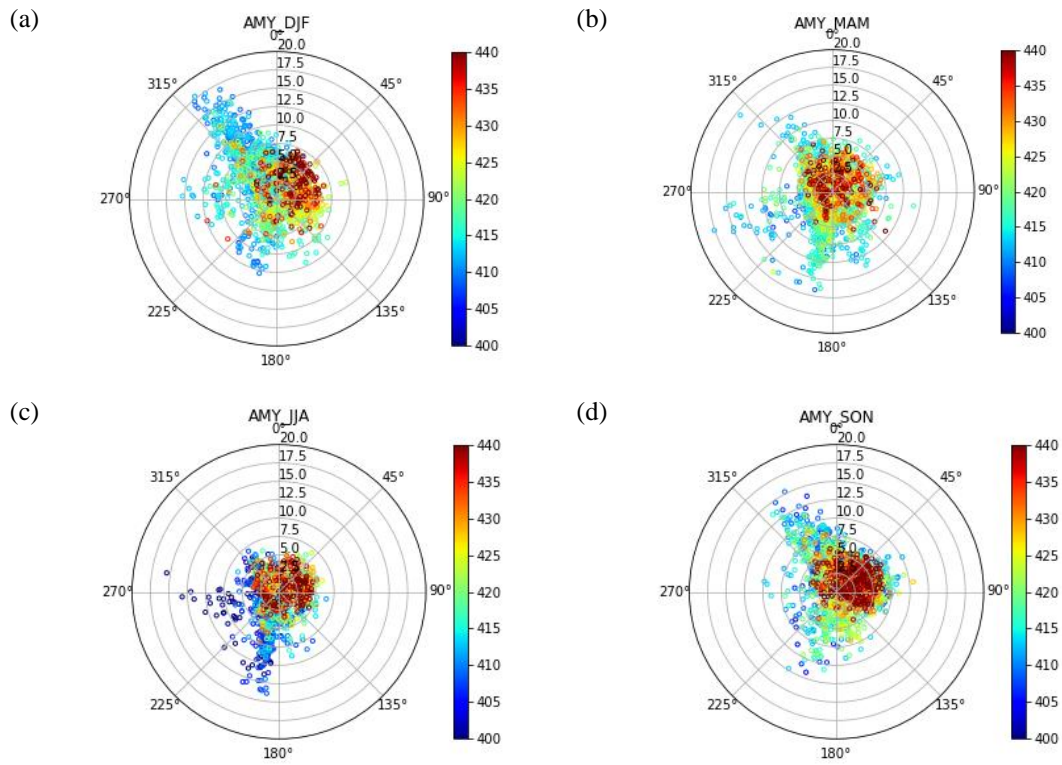
Figure 4. Bivariate polar plots for observed CO_2 (L1) in winter (a), spring (b), summer (c), and autumn (d) at AMY in 2016
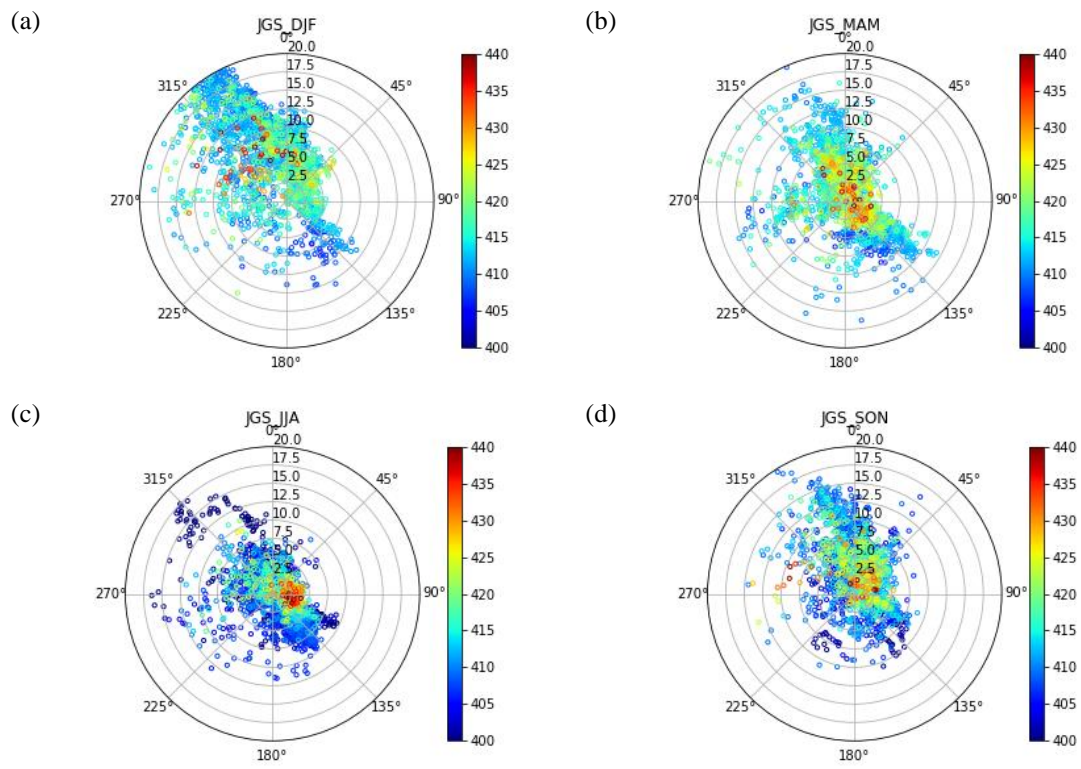
Figure 5. Bivariate polar plots for observed CO_2 (L1) in winter (a), spring (b), summer (c), and autumn (d) at JGS in 2016
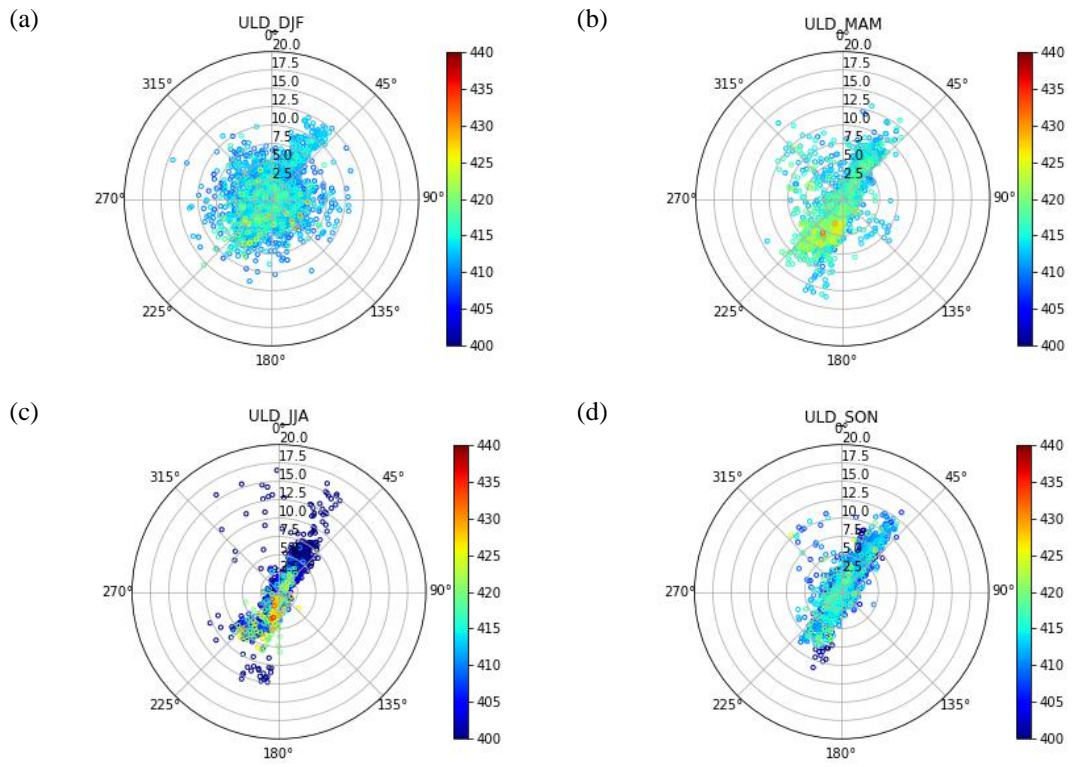
Figure 6. Bivariate polar plots for observed CO_2 (L1) in winter (a), spring (b), summer (c), and autumn (d) at ULD in 2016

(a)

(b)

(c)
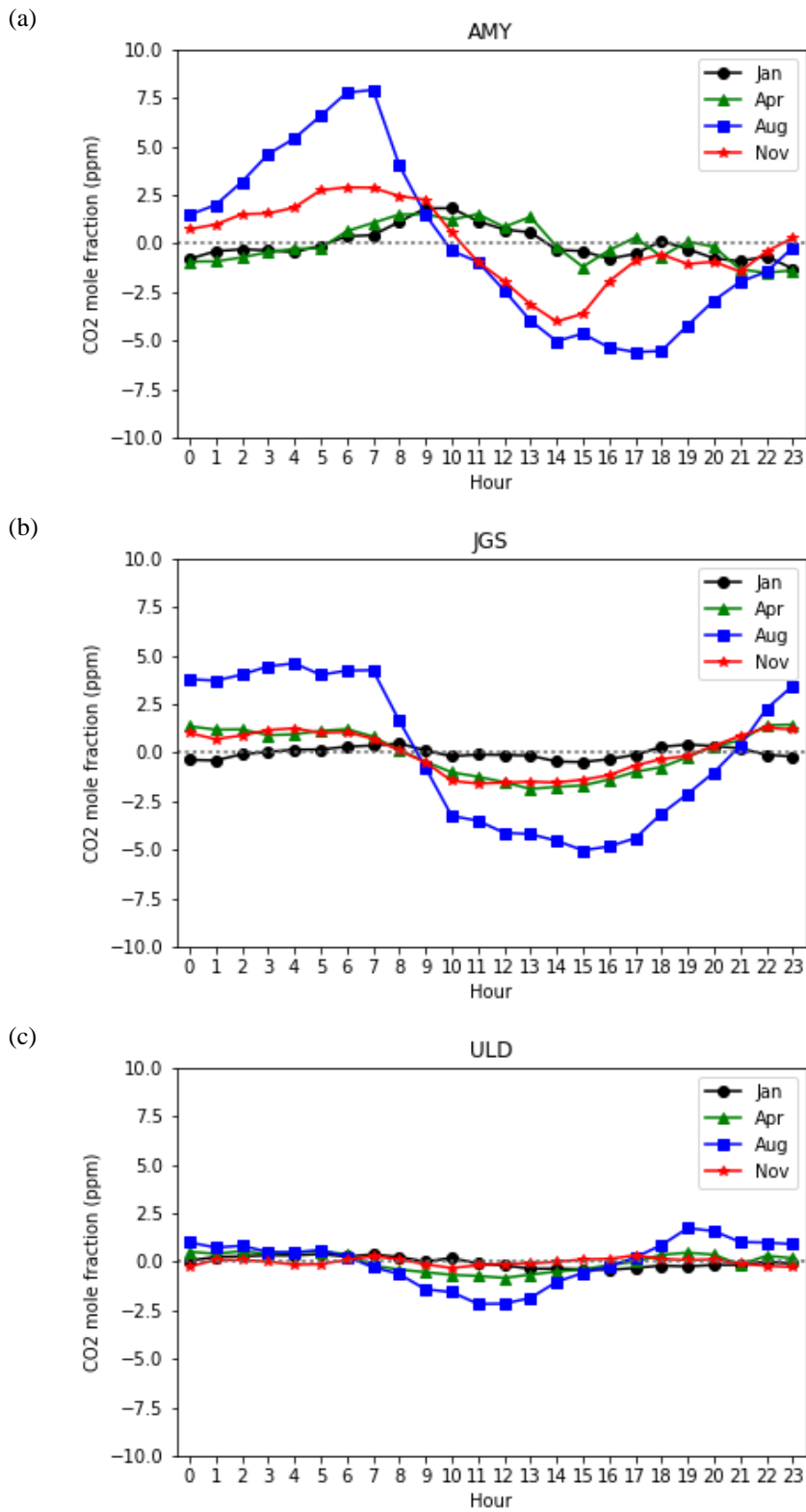
Figure 7. Mean diurnal variations of CO_2 mole fraction. Values show the average departure from the daily mean in January, April, August and November at (a) AMY, (b) JGS and (c) ULD from 2012 to 2016.

(a) (b)
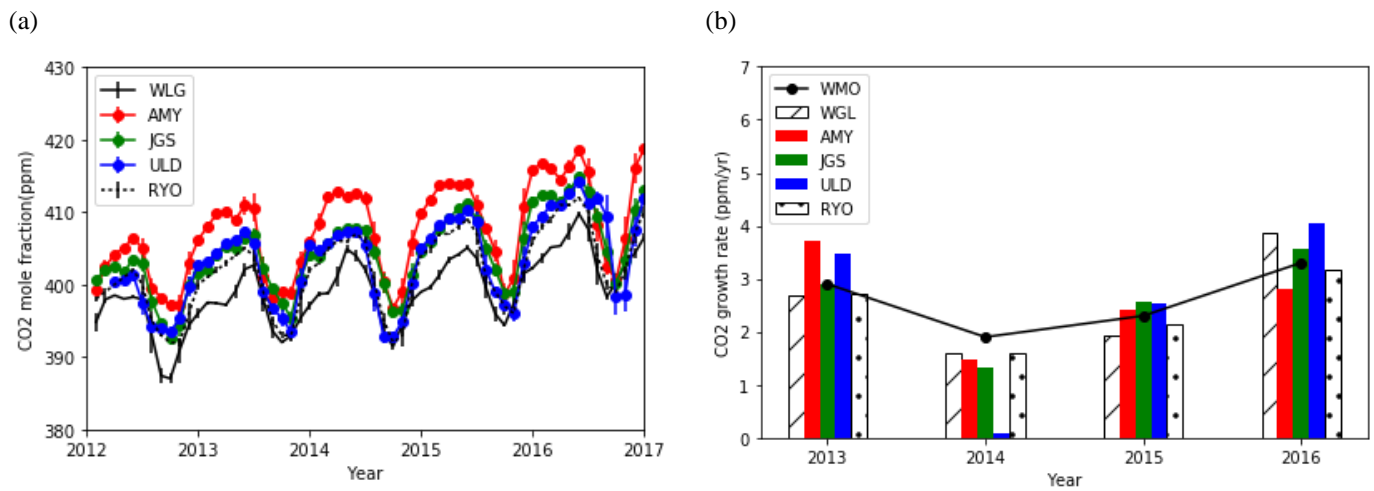
Figure 8. The time series of (a) the monthly mean CO_2 and (b) the annual growth rate at WLG, AMY, JGS, ULD and RYO. Annual growth rate was defined as the increase in the annual mean of de-seasonal (long term trend) values from the corresponding value in the previous year. The growth rate reported by WMO is overlaid on (b) and this value is annual increase (not de-seasonal), absolute differences from the previous year.
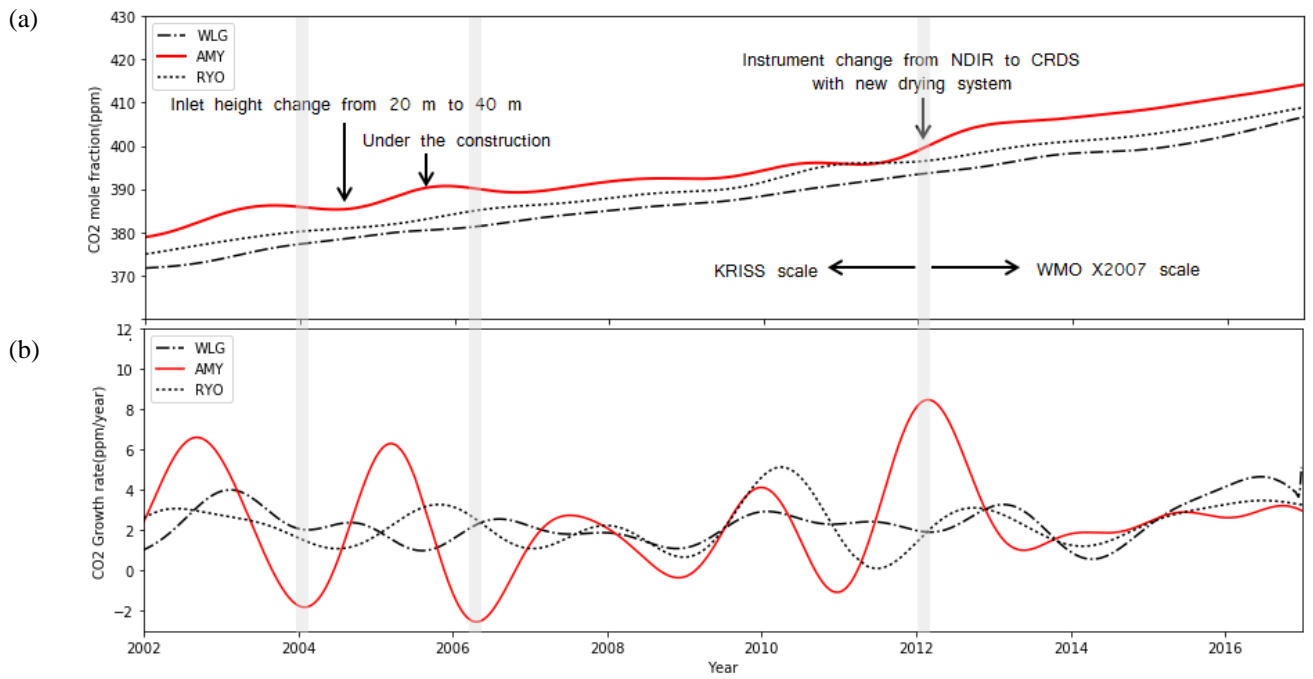
Figure 9. (a) Long-term trend of atmospheric CO_2 and its (b) instantaneous growth rate at WLG, AMY and RYO. Overlaid grey line indicated the period of the negative (in 2004 and 2006) and positive (in 2012) growth rates at AMY compared to other two East Asia stations (WLG and RYO).

Table 1. Information about the three KMA monitoring stations in Korea and the two monitoring stations in East Asia

Station	ID	Longitude	Latitude	Altitude	Inlet height	Measurement History
Anmyeondo, Korea	AMY	126.32°E	36.53°N	47 m	20 m	Since 1999 to July, 2004
					40 m	Since July, 2004
Jejudo Gosan Suwolbong, Korea	JGS	126.16°E	33.30°N	71.47 m	6 m	Since 2012
Ulleungdo*, Korea	ULD	130.90°E	37.48°N	220.9 m	10 m	Since 2012
Mt.Waliguan, China	WLG	100.90°E	36.28°N	3810 m	5 m	Since 1990
Ryori, Japan	RYO	141.82°E	39.03°N	260 m	20 m	Since 1987

*ULD is not GAW station.

Table 2. The uncertainty estimates for measurements of CO_2 at each station from 2012 to 2016. Units are ppm. All terms are in the 68% confidence interval

Uncertainty factors	AMY	JGS	ULD
U_{h2o}	0.023	0.009	0.018
U_p	0.053	0.046	0.025
U_r	0.048	0.056	0.065
U_{sacle}	0.088	0.088	0.088
U_T	0.116	0.114	0.114

Table 3. Annual mean CO_2 mole fractions with standard deviations from 2012 to 2016, mean seasonal amplitudes and growth rates. Seasonal amplitudes are calculated from the detrended data. CO_2 at ULD, 2012 was calculated only from February to December, without January. Units are dry-air mole fractions (ppm)

Year	WLG	AMY	JGS	ULD	RYO
2012	394.7 ± 3.9	402.8 ± 3.6	399.7 ± 3.7	398.4 ± 3.6	397.6 ± 3.7
2013	397.2 ± 3.1	405.4 ± 4.6	402.5 ± 3.5	401.8 ± 4.4	400.1 ± 4.2
2014	398.6 ± 3.8	407.8 ± 5.7	403.9 ± 4.0	401.9 ± 5.5	401.7 ± 5.1
2015	401 ± 3.3	410.2 ± 5.7	407.0 ± 4.5	405.0 ± 5.0	404.1 ± 4.4
2016	404.9 ± 3.2	412.6 ± 6.1	410.0 ± 4.6	409.3 ± 5.1	407.4 ± 4.5
Mean seasonal amplitude over 5 years.	12.2 ± 0.9	15.4 ± 3.3	13.2 ± 1.7	14.2 ± 3.1	13.5 ± 1.6
Maximum	*5.4 ± 0.7*	*5.8 ± 0.7*	*4.8 ± 0.4*	*5.4 ± 1.0*	*5.6 ± 0.4*
Minimum	*-6.8 ± 0.7*	*-9.6 ± 2.6*	*-8.3 ± 1.3*	*-8.8 ± 2.3*	*-7.9 ± 1.3*
Mean annual growth rate over 5 years (ppm·yr^{-1})	2.5 ± 1.1	2.5 ± 0.7	2.6 ± 0.9	2.5 ± 1.7	2.4 ± 0.7